frontiers | Frontiers in Earth Science

ORIGINAL RESEARCH
published: 19 May 2022
doi: 10.3389/feart.2022.908899

Late Quaternary Activity: Kouma Fault

Weimin He, Leihua Wei, Shuya Xu, Senlin Wan, Jie Yang and Mingjun Liu*

Geophysical Exploration Center, China Earthquake Administration, Zhengzhou, China

The Kouma Fault, located at the northern foot of the Mangshan Mountain in Luoyang City, Henan Province, China, is an active fault newly discovered in the field seismic geological survey. The Kouma Fault is a normal fault that is approximately 30 km in length, near the east-west strike, and the north dip. The study on the nature of the Quaternary activity of the Kouma Fault is of great significance to the potential seismic source zone division, urban and rural land planning, site selection for major projects, the assessment and prevention of earthquake disaster risk. Through a series of seismic geological surveys, 12 fault outcrops were discovered, which were all distributed on the slopes of the loess gullies. The Kouma Fault cuts loess, clay, sand, and gravel. The fault planes and scratch can be seen clearly. The filling in the fault zone is dominated by clay, loess, and pebbles, among others. When the width of the fault zone is smaller (10–30 cm), most clay in the zone is laminated in occurrence. The laminated surface is almost parallel to the fault plane and the long axis direction of pebbles in the fault zone is almost parallel to the fault plane. When the width of the fault zone is greater (for instance, 1.6 m), the clay and loess in the fault zone are massive. The composite drilling geological section and trench reveal two paleoseismic events of the Kouma Fault, the paleoseismic event I occurred at the fault in the Middle Pleistocene; the paleoseismic event II occurred at the fault in the later period of the Late Pleistocene, and the vertical offset of the upper Pleistocene bottom boundary is 13.57 m. Based on the OSL age data in the fault G1 outcrop of the fault and TC1 and TC2 trenches, the latest activity age of the Kouma Fault may be defined within the range of (38.84 ± 4.69) to (40.90 ± 4.45) kaB.P. The latest active age of the Kouma fault is the late of Late Pleistocene. The average vertical slip rate of the fault during the Late Pleistocene has been 0.11 mm/a.

Keywords: active fault, trenching, composite drilling geological section, OSL, loess, Mangshan Mountain, Kouma fault

OPEN ACCESS

Edited by:
Hanchao Jiang,
China Earthquake Administration, China

Reviewed by:
Lichun Chen,
Guilin University of Technology, China
Ma Yinsheng,
Chinese Academy of Geologi-cal Sciences (CAGS), China
Mingjian Liang,
Independent researcher, China

****Correspondence:***
Weimin He
wmhe65@163.com

Specialty section:
This article was submitted to Structural Geology and Tectonics, a section of the journal Frontiers in Earth Science

Received: *31 March 2022*
Accepted: *02 May 2022*
Published: *19 May 2022*

Citation:
He W, Wei L, Xu S, Wan S, Yang J and Liu M (2022) Late Quaternary Activity: Kouma Fault. Front. Earth Sci. 10:908899. doi: 10.3389/feart.2022.908899

1 INTRODUCTION

The Kouma Fault is a newly discovered and named active fault by the seismic and geological survey works conducted in recent years, located at the northern foot of the Mang Mountain in Luoyang, Henan, China, and adjacent to the Yellow River in the northern direction (He, 2022). The Western Henan where the Kouma Fault is located features dense cities and towns, large populations, and a prosperous economy. The local people have high demands on their safety and prevention against earthquake disaster risks. It is of great significance for the division of potential hypocenters in Western Henan, urban and rural land planning, siting of significant projects, and evaluation, prevention, and control of earthquake disaster risks to research on the Late Quaternary activity of the Kouma Fault. The seismic and geological survey, trenching, drilling, and radiometric dating are substantial means to research on the fault activity, and abundant achievements have been obtained

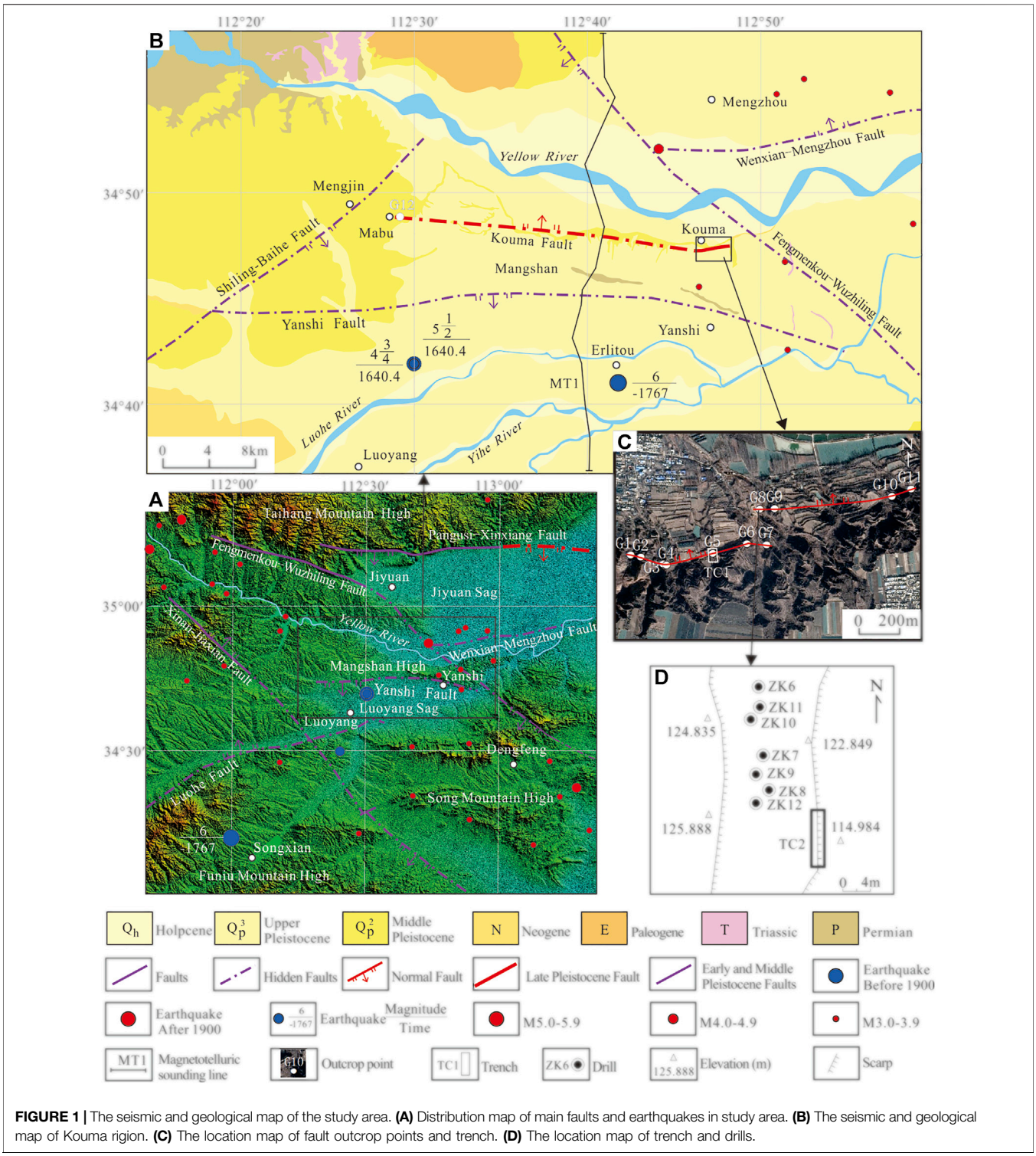

FIGURE 1 | The seismic and geological map of the study area. **(A)** Distribution map of main faults and earthquakes in study area. **(B)** The seismic and geological map of Kouma rigion. **(C)** The location map of fault outcrop points and trench. **(D)** The location map of trench and drills.

(Jiang et al., 2000; Ran et al., 2014a; Ran et al., 2014b; Ran et al., 2018; Wang et al., 2015; Min et al., 2016; Sun et al., 2016; Cao et al., 2018; Li et al., 2019). Some scholars (Wang et al., 2004; Pan et al., 2005; Bi et al., 2018; Ran et al., 2018; Li et al., 2020; Luo et al., 2020; Ma et al., 2020; Yu et al., 2020; Chang et al., 2021; Ha et al., 2021; Li et al., 2021; Liu et al., 2021; Lu et al., 2022; Shi et al., 2022) have established the loess-paleosol series of the Mang Mountain through research on loess and paleomagnetic test data of the mountain. Some scholars have obtained the occurrence of the Kouma Fault at the buried position (He, 2022), but the activity of the Kouma Fault is not demonstrated. Based on the seismic and geological survey, trenching, drilling, and radiometric dating,

among others, this study carries out comprehensive research on the Late Quaternary activity of the Kouma Fault, providing scientific evidence for earthquake prevention and disaster reduction in this region.

2 GEOLOGICAL SETTING

Kouma fault is surrounded by the Jiyuan sag on the north and Mangshan mountain on the south (**Figures 1A,B**). The south of Mangshan mountain is Luoyang sag. In the study area, the major Quaternary faults includ Xinan-Jiaxian fault, Fengmenkou-Wuzhiling fault, Luohe fault, Pangusi-Xinxiange fault, Yanshi fault, and Wenxian-Mengzhou fault. Among them, the Xinan-Jiaxian fault, the Fengmenkou-Wuzhiling fault, the Luohe fault, the Yanshi fault, the Pangusi-Xinxiange fault, and the Wenxian-Mengzhou fault are the early and middle Pleistocene faults. In addition, the last active times of the Pangusi-Xinxiang fault are the early and middle Pleistocene in the western section, the late Pleistocene in the middle section, and the early and middle Pleistocene in the eastern section (outside the figure) respectively. The Yanshi fault belongs to one of the northern marginal faults of the Luoyang sag.

The Kouma Fault is located in the western part of the Henan Province, China, which ranges from the Mabu Village, Mengjin County in the west to the Kouma Village, Mengjin County in the east. The Kouma Fault is a normal fault, with a strike of almost west-east, and a dip of the north (**Figure 1B**). The length of the Kouma Fault is calculated based on the distance from the outcrop of the fault at the most western end to that at the most eastern end, namely, and is approximately 30 km.

The Kouma fault is one of the southwest marginal faults of the Jiyuan sag, which is an inherited subsidence basin in the Mesozoic and Cenozoic, with a subsidence range of 6,000–9,000 m. The subsidence rate of Jiyuan sag has weakened since the Neogene and formed a tilted basin rising in the north and falling in the south, with the corresponding deposit thickness is 200–400 m.

The maximum historical earthquake in the study area is the 1767 B.C Yanshi Earthquake, which had a magnitude of 6 (**Figures 1A,B**).

3 MATERIAL AND METHODS

Using the method of seismic and geological survey, 12 fault outcrops (**Figures 1A,B**) have been found in the Kouma Fault through the seismic and geological survey, all of which are located on the slope of the loess gully. There are 11 outcrops (G1–G11) in the southeastern part of the Kouma Village, and there is one outcrop (G12) at the eastern part of the Mabu Village. Among them, the fault plane in some fault outcrops occurs in the valleys and steep cliffs, and those in other fault outcrops are covered by slope deposits that have to be exposed by manual excavation. The Kouma Fault cuts loess, clay, sand, and gravel. The fault planes and scratch can be seen clearly. From a top view, the Kouma fault is hidden in Malan loess. The typical fault outcrops are introduced hereunder.

The G5 and G8 outcrops of the fault with the existence of the Late Pleistocene loess (Malan Loess) were selected to carry out trenching work, and the numbers of the trenches are TC1 and TC2 (**Figures 1C,D**), respectively. After the excavation of every trench and leveling-down treatment of the trench wall, we hung the square grid line with a side length of 1 m on the surface of the trench wall, then carried out the measurement, geological record, photography, and age sampling and testing, and then carried out comprehensive research. The OSL age was tested at Key Laboratory of Crustal Dynamics, Institute of Crustal Dynamics, CEA, and the ESR age was tested at Measurement and Testing department of China Institute of Atomic Energy.

In TC1 and TC2 trenches, the equivalent stratum in the footwall (hanging wall) of the fault has not been revealed. The drilling survey was carried out on the hanging wall of the TC2 trench, and seven holes were drilled with a depth of 21–42 m (**Figure 1D**) to obtain the vertical fault throw and slip rate of the fault.

In order to detect the deep structure of the Kouma fault, a 48.36 km magnetotelluric sounding line named MT1, was arranged across the Kouma fault and Mangshan Mountain (**Figure 1B**). The V8 networked multi-function electrical instrument of Phoenix geophysical company of Canada was used for field data acquisition, and 14 broadband magnetotelluric sounding points were completed, of which 2 are inspection points. The collected frequency range is 320–0.000137 hz. Five electromagnetic field components of Ex, Ey, Hx, Hy, and Hz were collected on the magnetotelluric sounding points.

4 RESULTS

4.1 Seismic and Geological Survey

The typical fault outcrop points discovered through seismic and geological survey are introduced as follows.

4.1.1 G1 Outcrop of Fault

As shown in **Figures 2A–C**, the footwall (hanging wall) stratum revealed by the G1 outcrop of fault is almost consistent with the loess-paleosol series of the Mang Mountain (Wang et al., 2004). Among them, the U4 paleosol stratum is S11; the U11 loess stratum is L8, and the paleomagnetism B/M boundary located at the bottom of L8; the U16 paleosol stratum is S5; the U23 loess stratum is L2, where the age data of 1 OSL is (74.75 ± 8.79) ka.

The surface of the hanging wall (footwall) of the fault is the U13 loess stratum, where the age data of 1 OSL is (95.13 ± 10.67) ka (**Figure 2A**; **Table 1**). Subject to the offset impact of the fault, there are some missing points for the U22 paleosol stratum of the hanging wall of the fault located adjacent to the fault; the thickness of the U21 paleosol stratum varies greatly, and the paleosol stratum is up-warping towards the near-fault direction in terms of spatial distribution (**Figures 2A,B**).

The fault revealed by the G1 outcrop is a normal fault, and the fault plane and fault zone are clear (**Figures 2A–C**). The width at the middle-upper part of the fault is within the range of 2–8 cm, and the width at the lower part may reach 30 cm. The filling in the

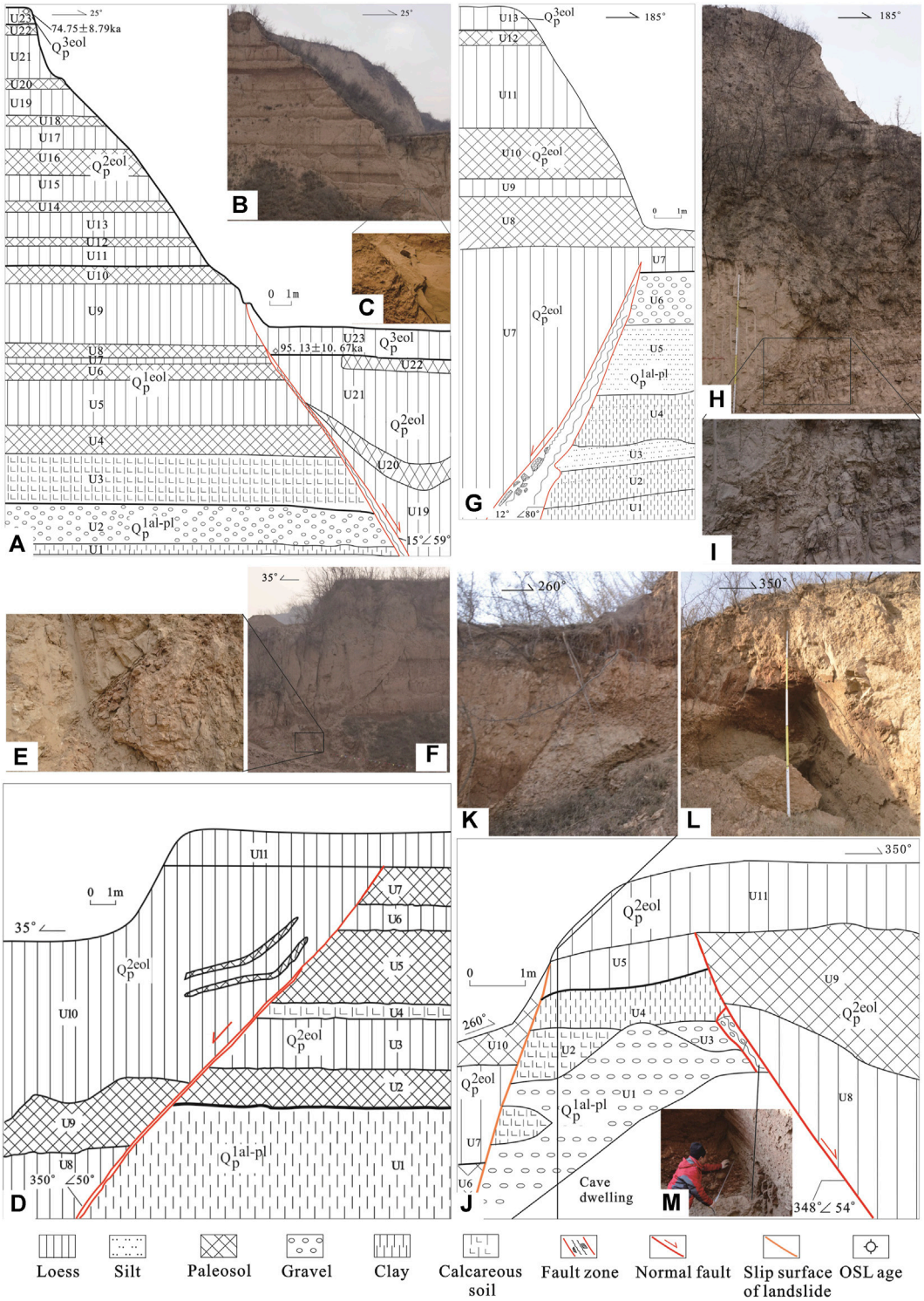

FIGURE 2 | The photographs and explanation of the typical outcrops of Kouma Fault. **(A)** The geological profile of G1 outcrop. **(B)** The panoramic photographs of G1. **(C)** The photographs of fault zone of G1 outcrop. **(D)** The geological profile of G2 outcrop. **(E)** The photographs of fault zone of G2 outcrop. **(F)** The panoramic photographs of G2. **(G)**The eological profile of G3 outcrop. **(H)** The panoramic photographs of G3. **(I)** The photographs of fault zone of G3 outcrop. **(J)** The geological profile of G6 outcrop. **(K)** The photographs on the left of G6. **(L)** The photographs on the middle and right of G6. **(M)** The photographs of fault zone of G6 outcrop.

TABLE 1 | OSL dating results of the Kouma Fault.

Sampling Site	Laboratory Number	Testing Method	U (μg/g)	Th (μg/g)	K (%)	Water Content (%)	Environmental Dose Rate (Gy/Ka)	Equivalent Dose (Gy)	Age (Ka)
G1	19-OSL-250	SMAR	2.27	11.20	1.75	3.78	3.81 ± 0.28	284.43 ± 25.81	74.75 ± 8.79
G1	19-OSL-251	SMAR	2.21	11.60	1.79	5.14	3.79 ± 0.28	360.63 ± 30.43	95.13 ± 10.67
TC1	18-OSL-182	SMAR	2.34	10.00	1.95	2.39	4.02 ± 0.31	178.67 ± 13.71	44.49 ± 4.81
TC1	18-OSL-182r	SMAR	2.34	10.00	1.95	2.39	4.02 ± 0.31	162.07 ± 8.22	40.36 ± 3.70
TC1	18-OSL-183	SMAR	2.35	10.20	1.93	1.97	4.04 ± 0.31	156.86 ± 14.64	38.84 ± 4.69
TC1	19-OSL-242	SMAR	2.01	11.50	1.87	6.55	3.65 ± 0.27	292.62 ± 30.62	80.22 ± 10.32
TC1	19-OSL-243	SMAR	2.08	10.90	1.62	5.89	3.40 ± 0.25	233.38 ± 19.07	68.59 ± 7.60
TC1	19-OSL-244	SMAR	2.36	11.40	1.84	1.26	4.01 ± 0.31	257.12 ± 18.93	64.19 ± 6.90
TC2	18-OSL-178	SMAR	2.26	10.10	1.96	2.68	3.85 ± 0.30	161.73 ± 7.37	42.06 ± 3.83
TC2	18-OSL-178r	SMAR	2.26	10.10	1.96	2.68	3.85 ± 0.30	168.58 ± 9.42	43.84 ± 4.24
TC2	18-OSL-180	SMAR	2.36	10.90	2.02	2.49	4.10 ± 0.32	228.11 ± 24.72	55.63 ± 7.42
TC2	18-OSL-181	SMAR	2.33	11.00	2.01	3.74	4.03 ± 0.31	215.87 ± 16.89	53.55 ± 5.86
TC2	19-OSL-246	SMAR	2.61	10.80	1.81	5.01	3.78 ± 0.28	304.34 ± 22.67	80.51 ± 8.56
TC2	19-OSL-247	SMAR	2.10	8.75	1.63	4.41	3.27 ± 0.25	222.53 ± 18.98	68.15 ± 7.82
TC2	19-OSL-248	SMAR	2.54	10.80	1.81	1.44	3.99 ± 0.31	163.3 ± 12.44	40.90 ± 4.45

fault zone is dominated by the grayish-yellow and yellowish-brown loess, which is massive. The latest stratum offset by the fault is the loess at the U23 stratum, and the overlying stratum is lacking above the fault up-break point.

At the G1 outcrop of the fault, the measured occurrence of the fault plane is 15°∠59°.

4.1.2 G2 Outcrop of Fault

As shown in **Figure 2D**, the footwall stratum of the fault revealed by the G2 outcrop of the fault is the Lower Pleistocene Series clay stratum, and the Middle Pleistocene Series paleosol stratum and loess stratum. The hanging wall stratum of the fault is the Middle Pleistocene Series paleosol stratum and loess stratum. Among them, the thickness of the U9 paleosol stratum varies greatly; there are two pieces of paleosol belts in the U10 loess stratum, the upper part of which is spread approximately in parallel with the fault plane, and the lower part of which has less inclination. The spatial spread shape of the paleosol belt in the U10 loess stratum is related to the offset activity of the fault.

The fault revealed by the G2 outcrop fault is a normal fault, and the fault plane and fault zone are clear (**Figures 2D–F**). The width of the fault zone is within the range of 10–20 cm. The fault zone becomes convergent upwards and narrows down, and then pinches out at the bottom of the U11 loess stratum of the Middle Pleistocene Series. The filling of the fault zone is dominated by red clay and yellowish-brown loess, which are laminated in occurrence. The laminated surface is distributed almost in parallel with the fault plane.

The G2 outcrop reveals that the latest active age of the fault is the Middle Pleistocene. At the G2 outcrop of the fault, the measured occurrence of the fault plane is 350°∠50°.

4.1.3 G3 Outcrop of Fault

As shown in **Figure 2G**, the footwall stratum of the fault revealed by the G3 outcrop of fault is the clay, silty-sand, and pebble stratum of the Lower Pleistocene Series. The hanging wall stratum of the fault is the Middle Pleistocene Series paleosol stratum and loess stratum.

The fault revealed by the G3 outcrop is a normal fault, and the fault plane and fault zone are clear (**Figures 2G–I**). The width of the lower part of the fault zone is 1.6 m and the fault zone becomes convergent upwards and narrows down. Subject to the blocking effect of slope surface deposits at the upper part of the fault outcrop, the location of the fault up-breakpoint is relatively fuzzy. According to the preliminary judgment, the fault up-breakpoint will pinch out upwards on top of the U7 loess stratum of the Middle Pleistocene Series. The filling in the fault zone is dominated by the grayish-yellow, which is massive; it contains the purple-red clay mass, whose surface is developed with the grayish-black ferromanganese thin film. It contains a few pebbles with good roundness and also contains the grayish-white calcium mass, grayish-yellow, and grayish-green silty sand mass.

The G3 outcrop reveals that the latest active age of the fault is the Middle Pleistocene. At the G3 outcrop of the fault, the measured occurrence of the fault plane is 12°∠80°.

Therefore, the G3 outcrop of fault is covered by the slope surface deposits of loess valleys, which are exposed by manual excavation only.

4.1.4 G6 Outcrop of the Fault

As shown in **Figure 2J**, the footwall stratum of the fault revealed by the G6 outcrop of fault is pebble, calcium soil, clay, paleosol, and loess clay stratum of the Lower Pleistocene Series. The hanging wall stratum of the fault is the Middle Pleistocene Series paleosol stratum and loess stratum.

The fault revealed by the G6 outcrop is a normal fault, and the fault plane and fault zone are clear (**Figures 2J–M**). The width of the upper part of the fault zone is 20 cm, and the fault zone pinches out upwards at the bottom of the U11 loess stratum of the

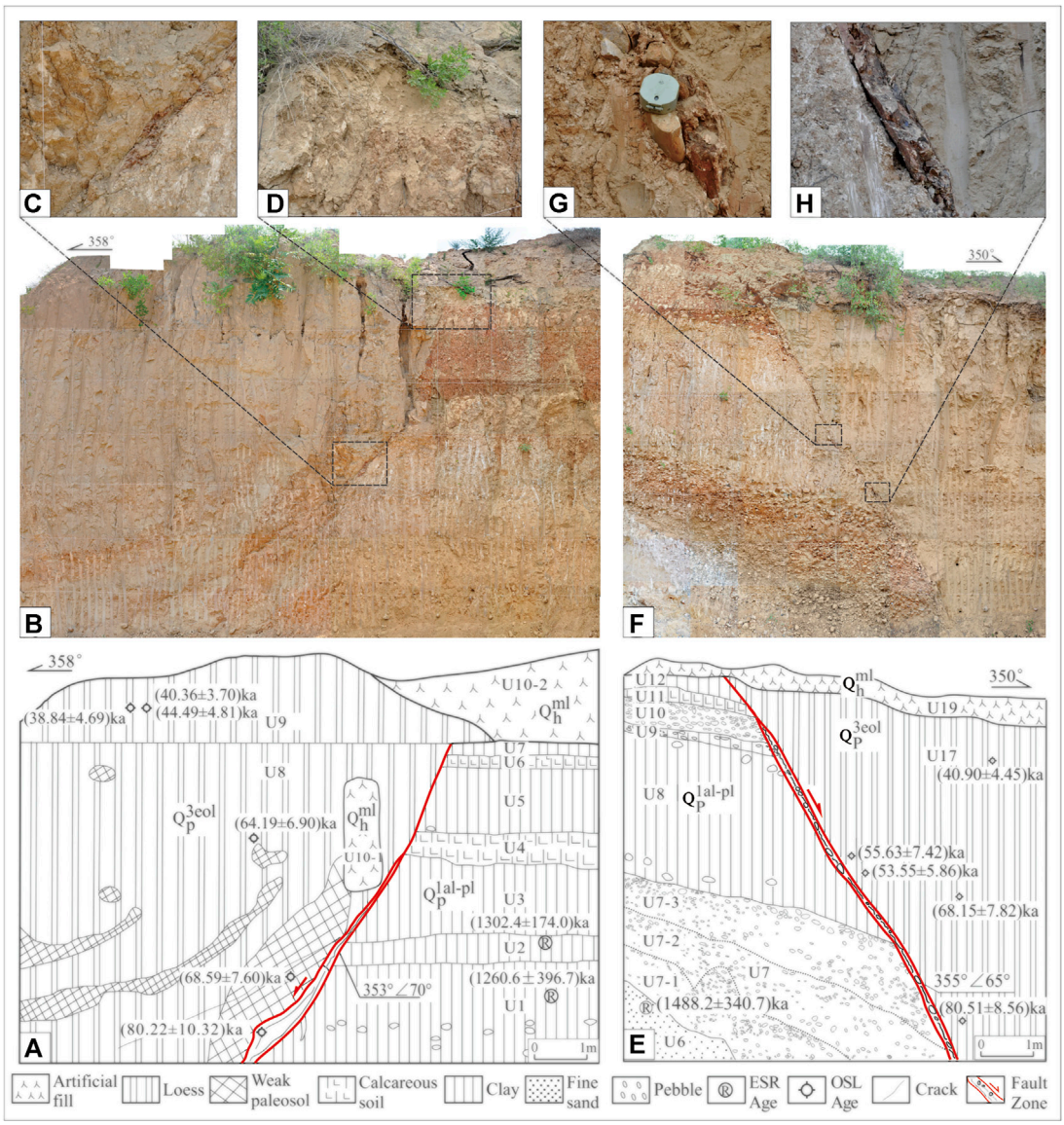

FIGURE 3 | The photographs and explanation of TC1 Trench (Left) and TC2 Trench (Right) of Kouma Fault. **(A)** The geological profile of TC1 trench. **(B)** The splicing photograph of TC1 trench. **(C)** The photograph of fault zone of TC1 trench. **(D)** The photograph of up-break point of TC1 trench. **(E)** The geological profile of TC2 trench. **(F)** The splicing photograph of TC2 trench. **(G)** The photograph of fault zone of TC2 trench. **(H)** The photograph of fault zone of TC2 trench.

Middle Pleistocene Series. The filling in the fault zone is dominated by the brownish red loess, which is massive but includes a few pebbles. The upper fault plane is brownish-red, and the striations of the fault are clear and longitudinal.

The G6 outcrop reveals that the latest active age of the fault is the Middle Pleistocene. At the G6 outcrop of the fault, the measured occurrence of the fault plane is 348°∠54°.

Notably, a landslide exists on the left side of the G6 outcrop of the fault (**Figure 2K**), and the landslide body consists of the U6 paleosol stratum, the U7 loess stratum, and the U10 paleosol stratum. Seemingly, this landslide looks like a normal fault, which is prone to cause misjudgment. The landslide body is located at the slope of the loess valley, namely, the free face, and the sliding surface of the landslide is almost in parallel with the slope surface of the loess valley.

4.2 Trenching

4.2.1 TC1 Trench

The TC1 trench is 11 m long and 6.4–8.8 m high (deep). See **Figure 3A** for the geological section of the trench wall and **Figure 3B** for the splicing photos of the trench wall. See **Table 2** for the main strata revealed by the TC1 trench, **Table 1** for OSL age data, and **Table 3** for ESR age data.

In the U8 stratum of the hanging wall, the grain size of weak paleosol mass ranges from 1 to 3 cm (smaller ones) to 30–40 cm (larger ones), and they are distributed in the grayish-yellow loess

TABLE 2 | Main strata revealed by TC1 trench.

Number of Stratum	Lithology	Geological Description	Geological Age and Origin Type	Location of Stratum
U1	Clay	It is yellowish brown, and contains the grayish white caliche nodules and grayish black ferromanganese nodules, and a few pebbles distributed in the shape of scattered beads (the mother rock is purple-red sandy rock) with the particle size of 3–8 cm, in the ellipsoidal shape, and with its surface being enveloped by the white grayish white calcium content; the soil texture is hard. A ESR sample age: (1,260.6 ± 396.7) ka	Q_p^{1al-pl}	Footwall stratum of the fault
U2	Clay	It is yellowish brown, and contains the grayish white caliche nodules and a few grayish black ferromanganese spots; the soil texture is hard. A ESR sample age: (1,302.4 ± 174.0) ka	Q_p^{1al-pl}	
U3	Clay	It is light grayish white and contains a great number of grayish white caliche nodules; the soil texture is hard	Q_p^{1al-pl}	
U4	Calcium soil	It is grayish white, and has the square structure, and the vertical fissure is developed; the soil texture is hard	Q_p^{1al-pl}	
U5	Clay	It is brownish red, and has the square structure, grayish black ferromanganese thin film and a few caliche nodules, and the pebbles with the grain size of 10–15 cm are occasionally found; the soil texture is hard	Q_p^{1al-pl}	
U6	Calcium soil	It is grayish white, and has the short square-cylinder-shaped structure, and the vertical fissure is developed; the soil texture is hard	Q_p^{1al-pl}	
U7	Clay	It is brownish red, and has the square structure, grayish black ferromanganese thin film and a few caliche nodules; the soil texture is hard	Q_p^{1al-pl}	
U8	Loess	It is grayish yellow, and contains a few white snail shells and a few caliche nodules. It contains the light reddish brown weak paleosol masses or belts. Two OSL samples age: (64.19 ± 6.90) and (68.59 ± 7.60) ka	Q_p^{3eol}	Hanging wall stratum of the fault
U9	Loess	It is grayish yellow, and contains a few white snail shells and a few caliche nodules. Three OSL samples age: (38.84 ± 4.69), (44.49 ± 4.81), and (40.36 ± 3.70) ka	Q_p^{3eol}	Hanging wall stratum of the fault
U10-1	Artificial fill	It is dominated by the grayish yellow loess, which is the artificially deposited soil. The greenish gray tiles may be found at bottom, the soil texture is loose, and the large pore may be found	Q_h^{ml}	Overlying stratum of the fault
U10-2	Artificial fill	It is dominated by the grayish yellow loess, which is the artificially deposited soil on the surface. The tree roots may be found, and the soil texture is loose. It is piled up by manual excavation	Q_h^{ml}	Overlying stratum of the fault

in the shape of scattered beads, and the weak paleosol belt is spread approximately in parallel with the fault plane; alternatively, its lower end is arc-shaped, extends northwards, and gradually levels off (**Figure 3A**); the spatial distribution characteristics of the weak paleosol mass or belt are caused by the offset of the fault.

The fault revealed by the TC1 trench is a normal fault, with a clear fault plane and fault zone (**Figures 3A–D**). The fault zone is generally wide at the bottom and narrow at the top, becomes convergent upwards, and then narrows down on top of the U8 loess stratum (**Figures 3B,D**), meaning the upper breakpoint of the fault is located on top of the U8 loess stratum. The overlying stratum of the up-breakpoint is the U9 loess stratum. The ages of three OSL samples are (38.84 ± 4.69), (44.49 ± 4.81), (40.36 ± 3.70) ka, respectively (**Figure 3A**; **Tables 1**, **2**). The latest active age of the fault is the late of Late Pleistocene revealed by TC1 trench. The width of the middle-up part of the fault zone is within the range of 5–10 cm. The filling is dominated by clay, which is reddish-brown, and laminated in occurrence. The laminated surface of the filling is distributed almost in parallel with the fault plane (**Figures 3B,C**). The striations on the fault plane are clear and almost vertical to the strike line of the fault plane. The

TABLE 3 | ESR dating results of the kouma Fault.

Sampling Site	Sample Serial Number	Annual dose (Gy·ka^{-1})	Paleo dose (Gy)	Age (ka)
TC1	KM-TC1-ESR-01	2.89	3,645 ± 1,147	1,260.6 ± 396.7
TC1	KM-TC1-ESR-02	3.41	4,447 ± 594	1,302.4 ± 174.0
TC2	KM-TC2-ESR-01	2.65	3,940 ± 902	1,488.2 ± 340.7
ZK11	KM-ZK11-ESR-03	3.55	3,588 ± 806	1,011.9 ± 227.3
ZK11	KM-ZK11-ESR-04	3.19	4,262 ± 725	1,337.7 ± 227.6

TABLE 4 | Main Strata Revealed byTC2 Trench.

Number of Stratum	Lithology	Geological Description	Geological Age and Origin Type	Location of Stratum
U6	Fine sand	It is off-white and contains the grayish white calcium mass and clay mass; the sand texture is loose. A ESR sample age: (1,488.2 ± 340.7) ka	Q_p^{1al-pl}	Footwall stratum of the fault
U7-1	Pebble	The pebble surface is enveloped by the grayish white calcium, most of pebbles have the grain size of 3–5 cm, a few of pebbles have the grain size of 10–15 cm; the mother rock is dominated by the greenish gray sandstone and a few mother rocks are purple-red sandstone, and they have good roundness and ellipsoidal shape; the filling is dominated by the light gray silty sands and is rich in calcium content; the local semi-cementation is found	Q_p^{1al-pl}	
U7-2	Pebble	Most of pebbles have the grain size of 2–4 cm, a few of pebbles have the grain size of 10–20 cm, and they have good roundness and ellipsoidal shape; the mother rock is dominated by the greenish gray sandstone; the filling is dominated by the reddish brown clay and contains the gray medium-fine sand and a few calcium masses; it is dense	Q_p^{1al-pl}	
U7-3	Pebble	The pebble surface is enveloped by the white calcium, most of pebbles have the grain size of 2–5 cm, a few of pebbles have the grain size of 10–20 cm, and they have good roundness and ellipsoidal shape; the mother rock is dominated by the greenish gray sandstone; the filling is dominated by the reddish brown clay and contains the calcium content; it is dense	Q_p^{1al-pl}	
U8	Clay	It is grayish yellow, and the grayish white calcium content is high. It contains a few pebbles (with the grain size of 10–15 cm), they have good roundness and ellipsoidal shape, and they are scattered at top and bottom of the stratum	Q_p^{1al-pl}	
U9	Clay	It is brownish red and contains the grayish white caliche nodules; the soil texture is hard. It contains the pebbles (with the grain size of 10–20 cm), and they have good roundness and ellipsoidal shape	Q_p^{1al-pl}	
U10	Pebble	The pebbles have the grain size of 10–15 cm, and they have good roundness and ellipsoidal shape; the filling is dominated by the reddish brown clay and it is dense	Q_p^{1al-pl}	
U11	Calcium soil	It is grayish white, and has the square structure, and the vertical fissure is developed; the soil texture is hard	Q_p^{1al-pl}	
U12	Clay	It is brownish red and contains a few pebbles (with the grain size of 4–6 cm) and grayish black ferromanganese thin film, and has the square structure and the vertical fissure is developed; the soil texture is hard	Q_p^{1al-pl}	
U17	Loess	It is grayish yellow, and contains a few white snail shells and a few caliche nodules. Five ESR samples age: (40.90 ± 4.45), (55.63 ± 7.42), (53.55 ± 5.86), (68.15 ± 7.82), and (80.51 ± 8.56) ka	Q_p^{3eol}	Hanging wall stratum of the fault
U19	Artificial fill	It is dominated by the grayish yellow loess and reddish brown clay, and the ash pit is locally found, which is the artificial soil deposited on surface. The tree roots may be found, and the soil texture is loose	Q_h^{ml}	Overlying stratum of the fault

medium laminated clay of the fault zone is mainly developed by the clay in the hanging wall of the fault (footwall) during the offset process. The filling at the lower part of the fault zone is dominated by the loess, which is grayish-yellow and 40 cm wide (thick). It contains white caliche nodules and a brownish-red clay mass. The loess in the lower part of the fault zone is loess in the hanging wall (footwall) of the fault zone that is residual in the new fault zone during the offsetting process. The age of the loess OSL sample in the fault zone is (80.22 ± 10.32) ka, but it does not indicate the offsetting age of the fault. The main cause is that the loess at this location is not fully exposed during the offsetting process.

At the TC1 trench, the measured occurrence of the fault plane is 353°∠70°.

4.2.2 TC2 Trench

The TC2 trench is 8 m long and 8.0–8.6 m high (deep). See **Figure 3E** for the geological section of the trench wall and **Figure 3F** for the splicing photos of the trench wall. See **Table 4** for the main strata revealed by the TC2 trench.

It should be noted that: 1) the U7 stratum consists of the U7-1 stratum, U7-2 stratum, and U7-3 stratum. 2) There is a path on top of the TC2 trench, and a scarp at the height of 2.6–3.4 m above the road surface is located on the western side of the path (**Figure 1D**), which reveals the U18 loess stratum (**Figure 4**).

The fault revealed by the TC2 trench is a normal fault, and the fault plane and fault zone are clear (**Figures 3E–H**). The fault zone is generally wide at the bottom and narrow at the top, becomes convergent upwards and then narrows down on top of the U17 loess stratum (**Figures 3E,F**), that is, the overlying stratum of the upper breakpoint of the fault is the U18 loess stratum. The ages of two OSL samples are (42.06 ± 3.83) and (43.84 ± 4.24)ka, respectively (**Figure 4**; **Tables 1**, **5**). The latest active age of the fault is the late of Late Pleistocene revealed by TC2 trench. The width of the fault zone is within the range of

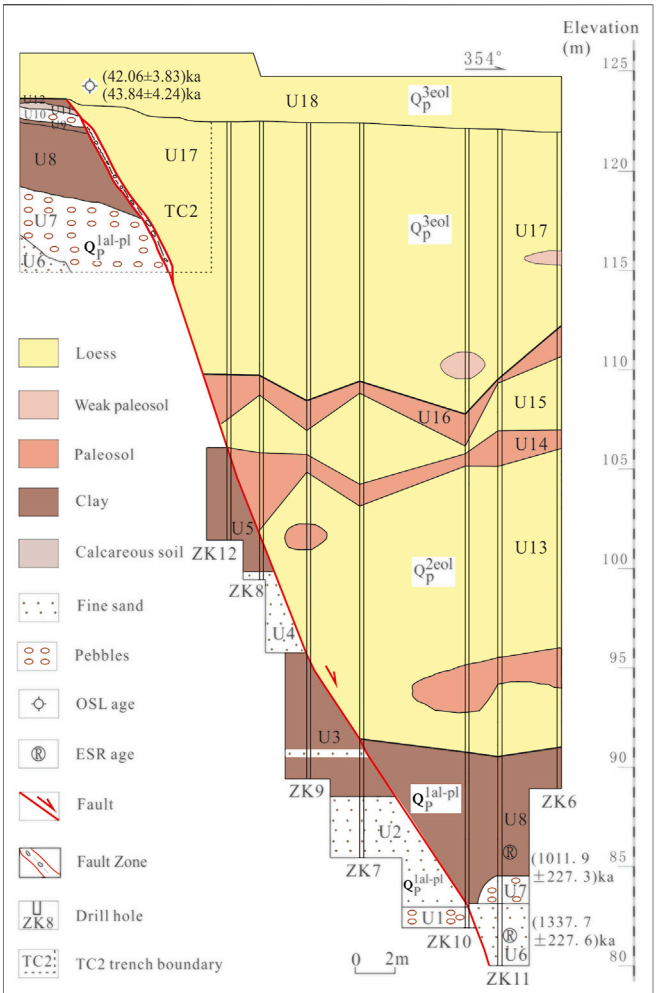

FIGURE 4 | The comprehensive interpretation map of trench and composite drilling geological section.

10–20 cm. The filling is dominated by clay, which is reddish-brown and dark-brown in color, and laminated in occurrence. The laminated surface of the filling is distributed almost in parallel with the fault plane (**Figure 3H**); the medium laminated clay of the fault zone is mainly developed by the clay in the hanging wall of the fault (footwall) during the offset process. The local filling is of pebble (with a grain size of 10–15 cm), and the long axis of the pebble is almost in parallel with the fault plane (**Figure 3G**). The fault zone contains the white calcium mass and laminated clay inclusive of grayish-black ferrimanganic content; the striations on the fault plane are clear and almost vertical to the strike line of the fault plane.

At the TC2 trench, the measured occurrence of the fault plane is 355°∠65°.

4.3 Drilling Survey

The obtained combined composite drilling geological section, the TC2 trench profile sketch, and the geological profile of the scarp on the western side of path on top of the TC2 trench (**Figure 1D**) were drawn together, as shown in **Figure 4**. The main strata revealed by the combined drilling geological profile are shown in **Table 5**.

As shown in **Figure 4**, the top interfaces of the U1 pebble stratum (in borehole ZK10), the U3 clay stratum (in boreholes ZK7 and ZK9), and the U5 clay stratum (in boreholes ZK8 and ZK12) are fault planes. On the top and bottom of the fault plane, the lithologic characteristics of the stratum in a borehole may vary greatly. The fault plane occurrence revealed by the drilling has a good consistency with that revealed by the TC2 trench (He, 2022).

The stratum surface of the hanging wall of the faults such as the U10 paleosol stratum, U11 loess stratum, and U12 paleosol stratum revealed by drilling are uneven; the paleosol mass and weak paleosol mass exist in the loess stratum. These phenomena are related to fault activity.

In terms of the ESR age data, the ESR age [(1,337.7 ± 227.6) ka] for the U6 fine sand stratum of the hanging wall of the fault revealed by drilling is closer to that [(1,488.2 ± 340.7) ka] for the U6 fine sand of the footwall of the fault revealed by TC2 trench. Through the comparison and analysis conducted in combination with the lithologic characteristics of the stratum, it is found that the U6 fine sand stratum, U7 pebble stratum, and U8 clay stratum of the hanging wall of the fault revealed by drilling (**Figure 4**; **Table 5**) are the equivalent strata (strata of the same age) with the U6 fine sand stratum, U7 pebble stratum and U8 clay (**Figure 3E**, **Figure 4**, **Table 4**) stratum of the footwall of the fault revealed by drilling, respectively.

According to the measurement of the composite drilling geological section and the TC2 trench, the elevation difference of the top interface of the U8 clay stratum (bottom interface of the U13 loess stratum) is 29.02 m, and the elevation difference of the bottom surface of the U17 loess stratum is 13.57 m.

4.4 Magnetotelluric Sounding

Non-linear Conjugate Gradient Inversion was used to process the magnetotelluric sounding data and the magnetotelluric two-dimensional electrical interpretation map was obtained (**Figure 5**). In the upper part of the profile with a depth of 5 km, the apparent resistivity value directly below Mangshan is significantly higher than that of Luoyang sag and Jiyuan sag on both sides. The Yanshi fault interpreted between Mangshan and Luoyang sag, is regarded as a normal fault apparent dipping to the south. Between Mangshan and Jiyuan sag, a fault can also be interpreted, named the Kouma fault, it is a normal fault with an apparent dip to the north. Mangshan is a bulge relative to Luoyang sag and Jiyuan sag. Mangshan is a bulge relative to Luoyang sag and Jiyuan sag, which form a horst structure.

5 DISCUSSION

5.1 Evidence of Kouma Fault

According to the seismic and geological survey, 12 Quaternary outcrops were discovered along the Kouma fault (**Figures 1B,C**, **2**). From the perspective of landform, there seems to be a loess landslide sliding northward (towards the Yellow River) at the

north edge of Mangshan Mountain in the southeast of Kouma village, however, through the investigation of all the Loess gullies developed in the north-south direction (some with a depth of 96 m), there is no sliding surface of landslide sliding in the north direction with steep upper part and gentle lower part. In addition, landslides sliding eastward (towards the gully) have also been discovered in the loess slopes on both sides of the Loess Gully (**Figures 2J,K**).

The composite drilling geological section located in the hanging wall of the Kouma fault also indicates the existence of the fault (**Figure 4**).

Magnetotelluric sounding MT1 section also reflects the existence of faults on the northern edge of Mangshan Mountain (**Figure 5C**).

Certainly, further work is needed on the research of Kouma fault, such as shallow seismic exploration and drilling.

5.2 Activity Analysis of the Kouma Fault

Through the above works such as trenching, drilling, and radiometric dating, among others, the composite drilling geological section and the TC2 trench reveal two paleoseismic events of the Kouma Fault (**Figure 6**).

Event I: In the Middle Pleistocene, the paleoseismic events occurred at the fault, and both the hanging wall and the footwall of the fault are the Middle Pleistocene stratum and the Lower Pleistocene stratum (**Figure 6A**). After the Middle Pleistocene stratum of the fault footwall was completely eroded, it accumulated the eolian loess of the Late Pleistocene (**Figure 6B**). In Event I, the vertical fault throw for the bottom interface of the Middle Pleistocene (the bottom interface of the U13 loess stratum in **Figure 4**) is 15.45 m.

Event II: In the later period of the Late Pleistocene, the paleoseismic events occurred to the fault again, which offset

TABLE 5 | Main strata revealed by drilling.

Number of Stratum	Lithology	Geological Description	Geological Age and Origin Type	Location of Stratum
U1	Pebble	The pebbles have the grain size of 10 cm, and they have good roundness and ellipsoidal shape; the mother rock is dominated by the quartz sandstone; the filling is dominated by the light yellow clay and contains the purple-red silty sands, blackish gray coarse sands and grayish white calcium content	Q_p^{1al-pl}	Footwall stratum of the fault
U2	Fine sand	It is brownish yellow and grayish yellow, and the calcium content is high	Q_p^{1al-pl}	
U3	Clay	It is light reddish brown and brown, and interlayered with the thin sand stratum, and also contains the grayish black ferromanganese mass, grayish white calcium mass and grayish green spot. The soil texture is hard, and the section is smooth and has the oily luster	Q_p^{1al-pl}	
U4	Fine sand	It is grayish white, and the calcium content is high	Q_p^{1al-pl}	
U5	Clay	It is light reddish brown and reddish brown, and contains the grayish white caliche nodules; it contains grayish green spots and grayish black ferromanganese thin films; the soil texture is hard, and the section is smooth and has the oily luster	Q_p^{1al-pl}	
U6	Fine sand	It is off-white and contains the grayish white calcium mass, and the clay content is high. A ESR sample age: (1,337.7 ± 227.6) ka	Q_p^{1al-pl}	Hanging wall stratum of the fault
U7	Pebble	The pebbles have the grain size of 5–10 cm, they have good roundness and ellipsoidal shape, the mother rock is dominated by the greenish gray sandstone, and the filing is the light reddish brown clay and gray fine sands, and contains the grayish white calcium content	Q_p^{1al-pl}	
U8	Clay	It is grayish yellow, and contains the grayish white caliche nodules and the caliche nodules are locally rich; the soil texture is hard, and the section is smooth and has the oily luster. A ESR sample age: (1,011.9 ± 227.3)ka	Q_p^{1al-pl}	
U13	Loess	It is yellowish brown and contains a few grayish black ferromanganese spots and a few grayish white caliche nodules with the grain size of about 2–8 cm, the reddish brown paleosol masses are interlayered	Q_p^{2al-pl}	
U14	Paleosol	It is brownish red, and contains a few grayish white caliche nodules, the grayish white calcium plinthitic stratum is locally developed, and it contains the grayish black ferromanganese spots; the soil texture is hard and the section is smooth	Q_p^{2al-pl}	
U15	Loess	It is brownish yellow, and contains the grayish white caliche nodules, the calcium is locally enriched, and the grain size of caliche nodule is within the range of 3–6 cm	Q_p^{2al-pl}	
U16	Paleosol	It is brownish red, and contains the grayish white caliche nodules and a few grayish black ferromanganese spots; the soil texture is hard and the section is smooth	Q_p^{2al-pl}	
U17	Loess	It is grayish yellow, and contains a few caliche nodules and a few white snail shells. It contains the light reddish brown weak paleosol masses	Q_p^{3eol}	
U18	Loess	It is grayish yellow, and contains a few white snail shells and a few caliche nodules. Two ESR samples age: (42.06 ± 3.83) and (43.84 ± 4.24) ka	Q_p^{3eol}	Overlying stratum of the fault

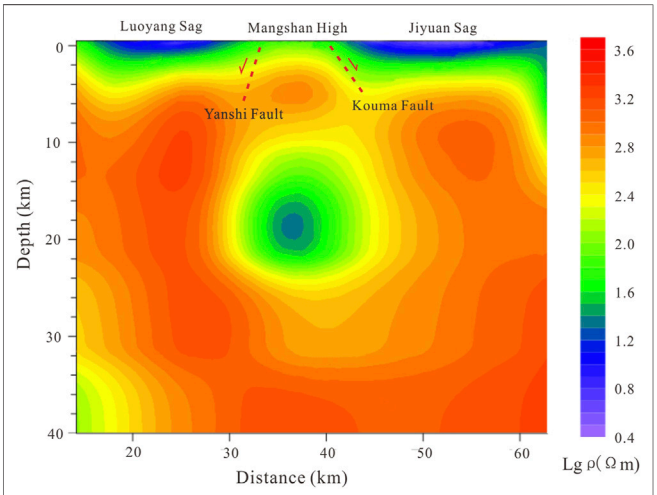

FIGURE 5 | The magnetotelluric two-dimensional electrical interpretation map.

the loess stratum of the Late Pleistocene (**Figure 6C**). After the fault scarp was completely eroded, it continued to accept the loess deposits of the Late Pleistocene (**Figure 6D**). Afterward, no further activity occurred to the fault. Subject to the effects of the loess slope erosion and human activities (for instance farming and road building), the present microgeomorphic landscape has been developed.

The faults zone revealed by TC2 trench is very clear (**Figures 3E,F**). The long axis of pebbles within the fault zone is basically parallel to the fault plane (**Figure 3G**), and the thin-layer clay is basically distributed parallel to the fault plane (**Figure 3H**). The fault zone is well preserved, it indicate that the time of fault dislocation (Paleoseismic event II) is the same as that of U17 loess sliding and covering the fault zone. The lithology and sedimentary age are completely different between U17 loess in the hanging wall of the fault and U7 pebble, U8 clay, U9 clay, U10 pebble, U11 calcareous soil, and U12 in the footwall of the fault (**Figures 3E,F** and **Figure 4**). In **Figure 4**, the weak paleosol mass in U17 layer could also be related to Paleoseismic event II. Paleoseismic event II is also revealed by TC1 trench and G1 fault outcrop.

It may be considered that paleoseismic events II have been revealed by the G1 outcrop of fault, TC1, and TC2 trenches, in view of the difference in sampling locations of OSL samples and the data errors of radiometric dating.

In the G1 outcrop of fault, the OSL sample age (74.75 ± 8.79) ka B.P in the latest offset, the U23 loess stratum can be used as the upper limit age data of the paleoseismic events II. In trial TC1 trench, the OSL sample age (64.19 ± 6.90) ka B.P in the latest U8 loess stratum offset by the fault may be used as the upper limit age data of the paleoseismic events II; the OSL sample age (38.84 ± 4.69) ka B.P, (40.36 ± 3.70) ka B.P and (44.49 ± 4.81) ka B.P in the overlying U9 loess stratum of the fault may be used as the lower limit age data of the paleoseismic events II. In trial TC2 trench, the OSL sample age (40.90 ± 4.45) ka B.P in the latest U17 loess stratum offset by the fault may be used as the upper limit age data of the paleoseismic events II; the OSL sample age (42.06 ± 3.83) and (43.84 ± 4.24) kaB.P in the overlying U18 loess stratum of the fault may be used as the lower limit age data of the paleoseismic events II. Based on these age data, the time of the paleoseismic events II may be defined within the range of (38.84 ± 4.69) to (40.90 ± 4.45) kaB.P (**Figure 7**). The latest active age of the Kouma fault is the late of Late Pleistocene.

In Paleoseismic event II, the vertical fault throw for the bottom interface of the Upper Pleistocene (the bottom interface of the U17 loess stratum in **Figure 4**) is 13.57 m, and the average vertical slip rate of the fault during the Late Pleistocene has been 0.11 mm/a.

5.3 The 1767 B.C. Yanshi Earthquake

The 1767 B.C. Yanshi earthquake had a magnitude of 6. According to "Historical strong earthquake catalog in China" (Department of earthquake disaster prevention, CEA, 1995), the 1767 B.C. Yanshi earthquake occurred in the southwest of Yanshi, Henan Province, with the epicenter (34.2°N, 112.0°E) near Song county (**Figure 1A**). Through the subsequent verification, Dong Ruishu (Dong et al., 2010) believes that the epicenter of the 1767 B.C. Yanshi earthquake is located at the Erlitou cultural site (the capital site of Xia Dynasty) in the south of Yanshi (**Figure 1B**).

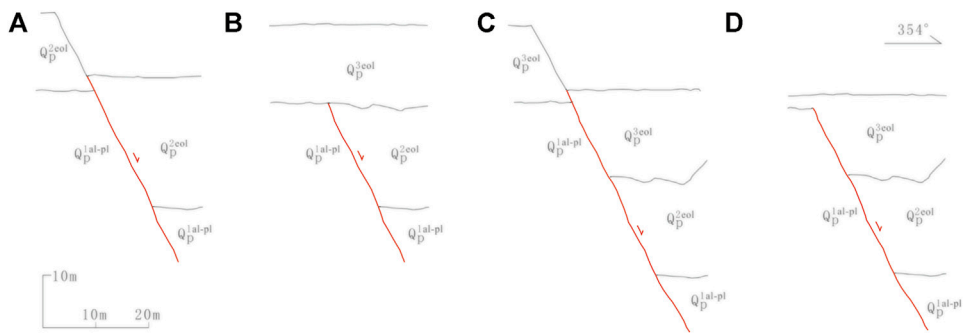

FIGURE 6 | (A) Schematic diagram of paleoseismic eventI. **(B)** Schematic diagram between paleoseismic eventI and paleoseismic eventII. **(C)** Schematic diagram of paleoseismic eventII. **(D)** Schematic diagram of present geological profile.

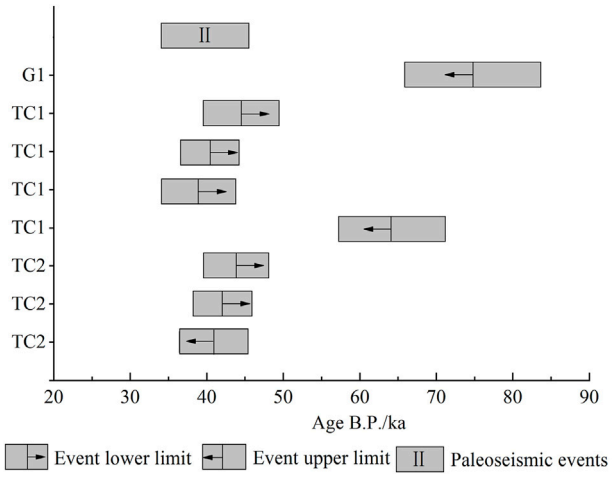

FIGURE 7 | The progessive constrained paleoseismic event in Kouma Fault.

The author considers that the seismotectonics of the 1767 B.C. Yanshi earthquake could related to the Kouma fault.

6 CONCLUSION AND SUGGESTIONS

(1) The Kouma Fault is a normal fault, with a dip of the north, a strike of almost east-west, and a length of approximately 30 km. As shown by the results obtained through the seismic and geological survey, trenching, drilling, radiometric dating, and comprehensive analysis—the paleoseismic events occurred at the fault in the Middle Pleistocene (event I); the paleoseismic events occurred at the fault again in the later period of the Late Pleistocene (event II). Based on the OSL age data in the G1 outcrop of the fault and the TC1 and TC2 trenches, the latest activity age of the Kouma Fault may be defined within the range of (38.84 ± 4.69) to (40.90 ± 4.45) kaB.P. The latest active age of the Kouma fault is the late of Late Pleistocene. The vertical fault throw for the bottom interface of the Upper Pleistocene (the bottom interface of the U13 loess stratum) of the Kouma Fault is 13.57 m, and the average vertical slip rate of the fault during the Late Pleistocene has been 0.11 mm/a.

(2) The filling in the fault zone of the Kouma Fault is dominated by clay, loess, and pebble, among others. When the width of the fault zone is smaller (10–30 cm), most clay in the fault zone is laminated in occurrence. The laminated surface is almost in parallel with the fault plane, and the long axis direction of pebbles in the fault zone is almost parallel to the fault plane. When the width of the fault zone is greater (for instance, 1.6 m), the clay and loess are massive.

(3) In the loess valley region, some outcrops of the fault are covered by slope deposits; the sliding surfaces of landslides on some loess valley side slopes are very similar to the sliding surfaces of the fault. They shall be carefully identified during the field geological survey process.

(4) Geological data is inadequate for the middle and deep part of the Kouma Fault, and it is recommended to carry out further research with shallow and deep seismic explorations, and to conduct the Kouma Fault seismic hazard evaluation based on those results.

DATA AVAILABILITY STATEMENT

The original contributions presented in the study are included in the article/Supplementary Material, further inquiries can be directed to the corresponding author.

AUTHOR CONTRIBUTIONS

WH is responsible for the overall implementation and writing papers. LW responsible for Seismic and Geological Survey and data analysis. SX responsible for geological graph drawing and paper finishing work. SW and JY participate in field operation drilling. ML has carried on the theory of technical guidance to the whole paper.

FUNDING

This study was supported by Spark Program of Earthquake Sciences (No. XH19060) and National Natural Science Foundation of China (No. 41704058).

ACKNOWLEDGMENTS

We are particularly grateful to Professor from Institute of Geology, CEA, China earthquake disaster prevention center and National institute of natural hazards, China for their helpful field guidance. We are also extremely grateful to Institute of Crustal Dynamics, CEA, and China Institute of Atomic Energy for their age test work.

REFERENCES

Bi, H., Zheng, W., Ge, W., Zhang, P., Zeng, J., and Yu, J. (2018). Constraining the Distribution of Vertical Slip on the South Heli Shan Fault (Northeastern Tibet) from High-Resolution Topographic Data. *J. Geophys. Res. Solid Earth* 123, 2484–2501. doi:10.1002/2017jb014901

Cao, Y., Ran, Y., Xu, H., Li, Y., Ma, X., Liang, M., et al. (2018). Holocene Activity of the Anqiu-Juxian Fault on the Jiangsu Segment of the Tanlu Fault Zone and its Tectonics Implication. *Chin. J. Geophys.* 61 (7), 2828–2844. (In Chinese with English abstract). doi:10.6038/cjg2018L0111

Chang, Z., Chang, H., Li, J., Mao, Z., and Zang, Y. (2021). Holocene Activity and Paleoearthquakes of the Weixi-Qiaohou Fault. *Seismol. Geol.* 43 (4),

881–898. (In Chinese with English abstract). doi:10.3969/j.issn.0253-4967.2021.04.009

Department of earthquake disaster prevention, CEA (1995). *Historical Strong Earthquake Catalog in China*. Beijing: Seismological Press. (In Chinese).

Dong, R., Yu, H., and Pan, B. (2010). Re-check of the 1767 B.C. Yanshi Earthquake, Henan Province. *Technol. Earthq. Disaster Prev.* 5 (4), 493–499. (In Chinese with English abstract). doi:10.3969/j.issn.1673-5722.2010.04.012

Ha, G., Ren, Z., Liu, J., Li, Z., Li, Z., Min, W., et al. (2021). New Discovery of Xiariha Fault Zone Around Dulan Area, Qinghai Province and its Tectonic Implications. *Seismol. Geol.* 43 (3), 614–629. (In Chinese with English abstract). doi:10.3969/j.issn.0253-4967.2021.03.009

He, W. (2022). Three-Point Method for Calculation of the Occurrence of Buried Active. *Fault* 46 (01), 36–47. (In Chinese with English abstract). doi:10.16539/j.ddgzyckx.2020.06.015

Jiang, W., Hou, Z., and Xiao, Z. (2000). Study on Paleoearthquakes of Qixinzhuang Trench at the XIadian Fault, Beijing Plain. *Seismol. Geol.* 22 (4), 413. (In Chinese with English abstract). doi:10.3969/j.issn.0253-4967.2000.04.010

Li, K., Xu, X., Wei, L., Wang, Q., and Shu, P. (2019). Evidence of Long Recurrence Times and Low Slip Rate along the 1668 Tancheng Earthquake Fault. *Chin. Sci. Bull.* 64 (11), 1168–1178. (In Chinese with English abstract). doi:10.1360/N972018-00961

Li, Z., Li, Y., Zhou, B., Zhu, G., liu, B., and Wu, J. (2021). New Insight on the Holocene Activity of the Eastern Marginal Fault of Daxing Uplift, Beijing Plain. *Seismol. Geol.* 43 (6), 1671–1681. (In Chinese with English abstract). doi:10.3969/j.issn.0253-4967.2021.06.018

Li, Z., Ren, Z., Liu, J., Ha, G., Li, Z., Wang, B., et al. (2020). New Discovery of Reshui-Taostuo River Fault in Dulan, Qinghai Province and its Implications. *Seismol. Geol.* 42 (1), 18–32. (In Chinese with English abstract). doi:10.3969/j.issn.0253-4967.2020.01.002

Liu, X., Yuan, D., Yao, Y., and Zou, X. (2021). Paleoearthquake Characteristics in Dunhuang Segment of the Sanweishan Fault. *Seismol. Geol.* 43 (6), 1398–1411. (In Chinese with English abstract). doi:10.3969/j.issn.0253-4967.2021.06.004

Lu, L., Zhou, Y., Zhang, P., and Cheng, X. (2022). Modelling Fault Scarp Degradation to Determine Earthquake History on the Muztagh Ata and Tahman Faults in the Chinese Pamir. *Front. Earth Sci.* 10 (9), 838866. doi:10.3389/feart.2022.838866

Luo, X., li, C., Ren, G., Li, X., Ma, Z., and Dong, J. (2020). The Late Quaternary Activity Features and Slip Rate of the Yanggao-Tianzhen Fault. *Seismol. Geol.* 42 (2), 399–413. (In Chinese with English abstract). doi:10.3969/j.issn.0253-4967.2020.02.010

Ma, J., Zhou, B., Wang, M., and An, L. (2020). Geological and Geomorphic Evidences for the Holocene Activity of the Nw Zheduotang Branch within the Xianshuihe Fault System. *Seismol. Geol.* 42 (5), 1021–1038. (In Chinese with English abstract). doi:10.3969/j.issn.0253-4967.2020.05.001

Min, W., Liu, Y., Chen, T., Shu, P., and Yu, Z. (2016). The Quantative Study on Activity of Dengdengshan-Chijiaciwo Faults Since Late Quaternary. *Seismol. Geol.* 38 (03), 503–522. (In Chinese with English abstract). doi:10.3969/j.issn.0253-4967.2016.03.002

Pan, B., Wang, J., Gao, H., Guan, Q., Wang, Y., Su, H., et al. (2005). Paleomagnetic Age of the Highest Terrace of the Yellow River in Kouma, Henan Province and its Indication to the Age of the Connection of the Yellow River. *Chin. Sci. Bull.* 50 (3), 255–261. (In Chinese). doi:10.1360/03wd0290

Ran, Y., Li, Y., Du, P., Chen, L., and Wang, H. (2014a). Key Techniques and Several Cases Analysis in Paleoseismic Studies in Mainland China(3):Rupture Characteristics, Environment Impact and Paleoseismic Indicators on Normal Faults. *Seismol. Geol.* 36 (02), 287–301. (In Chinese with English abstract). doi:10.3969/j.issn.0253-4976.2014.02.001

Ran, Y., Wang, H., Chen, L., Chen, W., Liang, M., and Xu, X. (2018). Late-Quaternary Fault Activity of the Longmen Shan Fault Zone-Evidence from Paleoseismic Trenching. *Chin. J. Geophys.* 61 (5), 1938–1948. (In Chinese with English abstract). doi:10.6038/cjg2018M0251

Ran, Y., Wang, H., Yang, H., and Xu, L. (2014b). Key Techniques and Several Cases Analysis in Paleoseismic Studies in Mainland China(4):Sampling and Event Analysis of Paleoseismic Dating Methods. *Seismol. Geol.* 36 (04), 939–955. (In Chinese with English abstract). doi:10.3969/j.issn.0253-4967.2014.04.001

Shi, F., He, H., Liu, Y., Wei, Z., and Sun, H. (2022). Active Tectonics of the Nantinghe Fault in Southeastern Tibetan Plateau and its Implications for Continental Collision. *Front. Earth Sci.* 9 (21), 818225. doi:10.3389/feart.2021.818225

Sun, H., He, H., Wei, Z., and Gao, W. (2016). The Quantative Study on Activity of Dengdengshan-Chijiaciwo Faults Since Late Quaternary. *Seismol. Geol.* 38 (03), 503–522. (In Chinese with English abstract). doi:10.3969/j.issn.0253-4967.2016.03.002

Wang, S., Jiang, F., Wu, X., Tian, G., Zhang, Z., Liu, A., et al. (2004). Loess Stratigraphy of Mangling in Henan Province. *J. Geomechanics* 7 (4), 309–314. (In Chinese with English abstract). doi:10.3969/j.issn.1006-6616.2001.04.004

Wang, Z., Wang, L., Xu, H., Ge, F., Yang, C., and Li, J. (2015). Geometric Feature and Latest Activities of the North Segment of the Anqiu-Juxian Fault. *Seismol. Geol.* 37 (1), 176–191. (In Chinese with English abstract). doi:10.3969/j.issn.0253-4967.2015.01.014

Yu, Z., Pan, H., Shen, J., Li, J., Zhang, M., and Dai, X. (2020). The Activity Features of Xiadian Fault Zone Revealed by Rongjiabao Trench and its Probabilistic Seismic Hazard Evaluation. *Seismol. Geol.* 42 (3), 688–702. (In Chinese with English abstract). doi:10.3969/j.issn.0253-4967.2020.03.010

Conflict of Interest: The authors declare that the research was conducted in the absence of any commercial or financial relationships that could be construed as a potential conflict of interest.